Structural and Kinetic Study of an Internal Substrate Binding Site in Dehaloperoxidase-Hemoglobin A from Amphitrite ornata

ARTICLE *in* BIOCHEMISTRY · MARCH 2013

Impact Factor: 3.02 · DOI: 10.1021/bi301307f · Source: PubMed

5 AUTHORS, INCLUDING:

Jing Zhao
North Carolina State University
7 PUBLICATIONS **26** CITATIONS
SEE PROFILE

Vesna de Serrano
North Carolina State University
18 PUBLICATIONS **356** CITATIONS
SEE PROFILE

BIOCHEMISTRY
including biophysical chemistry & molecular biology

Article

pubs.acs.org/biochemistry

Structural and Kinetic Study of an Internal Substrate Binding Site in Dehaloperoxidase-Hemoglobin A from *Amphitrite ornata*

Jing Zhao, Vesna de Serrano, Junjie Zhao, Peter Le, and Stefan Franzen*

Department of Chemistry, North Carolina State University, Raleigh, North Carolina 27695, United States

Supporting Information

ABSTRACT: X-ray crystal structures of dehaloperoxidase-hemoglobin A (DHP A) from *Amphitrite ornata* soaked with substrate, 2,4,6-tribromophenol (2,4,6-TBP), in buffer solvent with added methanol (MeOH), 2-propanol (2-PrOH), and dimethyl sulfoxide (DMSO) reveal an internal substrate binding site deep in the distal pocket above the α-edge of the heme that is distinct from the previously determined internal inhibitor binding site. The peroxidase function of DHP A has most often been studied using 2,4,6-trichlorophenol (2,4,6-TCP) as a substrate analogue because of the low solubility of 2,4,6-TBP in an aqueous buffer solution. Previous studies at low substrate concentrations pointed to the binding of substrate 2,4,6-TCP at an external site near the exterior heme β- or δ-edge as observed in the class of heme peroxidases. Here we report that the turnover frequencies of both substrates 2,4,6-TCP and 2,4,6-TBP deviate from Michaelis–Menten kinetics at high concentrations. The turnover frequency reaches a maximum in the range of 1400–1700 μM, with a decrease in rate at higher concentrations that is both substrate- and solvent-dependent. The X-ray crystal structure is consistent with the presence of an internal active site above the heme α-edge, in which the substrate would be oxidized in two consecutive steps inside the enzyme, followed by attack by H_2O via a water channel in the protein. The physiological role of the internal site may involve interactions with any of a number of aromatic toxins found in benthic ecosystems where *A. ornata* resides.

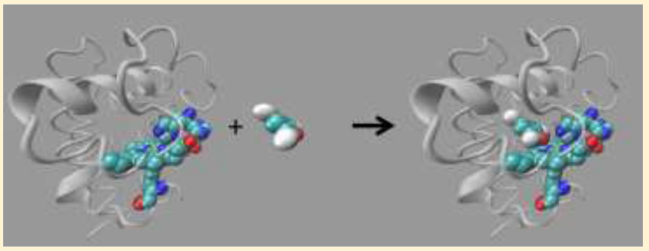

The bifunctional protein dehaloperoxidase-hemoglobin A (DHP A) from *Amphitrite ornata* is capable of oxidizing 2,4,6-tribromophenol (2,4,6-TBP) into 2,6-dibromoquinone (2,6-DBQ) in the presence of H_2O_2.[1] This chemical transformation is thought to be important for the survival of *A. ornata*, which does not synthesize 2,4,6-TBP but must survive in shallow coastal waters where other marine organisms produce this toxin.[2−5] There are two isoforms of DHP,[6] known as DHP A and B,[7] which are both capable of the peroxidase chemistry shown in Scheme 1. DHP B has an enzymatic rate 3 times greater than that of DHP A.[6] With the exception of our initial report of DHP A cloning,[8] subsequent studies have used 2,4,6-trichlorophenol (2,4,6-TCP) as a substrate analogue,[8−17] because the solubility of 2,4,6-TBP is so low in aqueous solvents that it is not practical for Michaelis–Menten kinetic measurements, NMR, or X-ray crystallographic determination of the binding site in aqueous buffer. The mechanism of oxidation of 2,4,6-TCP by DHP A involves two-site competitive inhibition, in which an inhibitor, 4-bromophenol (4-BP), binds at an internal site in the distal pocket perpendicular to the heme, while the substrate is presumed to bind at an external site near the heme β- or δ-edge (Figure 1, right panel).[13] The ionic strength effect and charged surface mutations show that there is a moderate electrostatic repulsion between the substrate and enzyme.[18] However, there are competing factors because the increasing pH, which increases the negative surface charge on both the enzyme and the substrate, leads to a greater product yield despite a decrease in the enzymatic rate.[10] An inactive cross-linked heme form known as compound RH competes with turnover at pH 5, but the internal delocalized radical mechanism that forms compound RH decreases significantly with an increasing pH.[19,20] At pH >6.5, an oxidized phenolic substrate on the protein surface (presumably near either the δ- or β-heme edge) leads to phenoxy radicals that diffuse away from the enzyme and react by disproportionation to form the quinone product,[11,13,21,22] which is a standard peroxidase mechanism.[23,24] Although it is considered the native substrate, the detailed physiology of 2,4,6-TBP in *A. ornata*, such as its diffusion and ultimate concentration in tissues, has not been reported. In our search for the native substrate binding site, we have used X-ray crystallography, based on the method of

Scheme 1. Basic Reaction for the Oxidation of 2,4,6-Trihalophenols by DHP

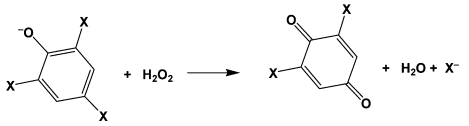

Received: September 26, 2012
Revised: March 9, 2013

   dx.doi.org/10.1021/bi301307f | *Biochemistry* XXXX, XXX, XXX–XXX

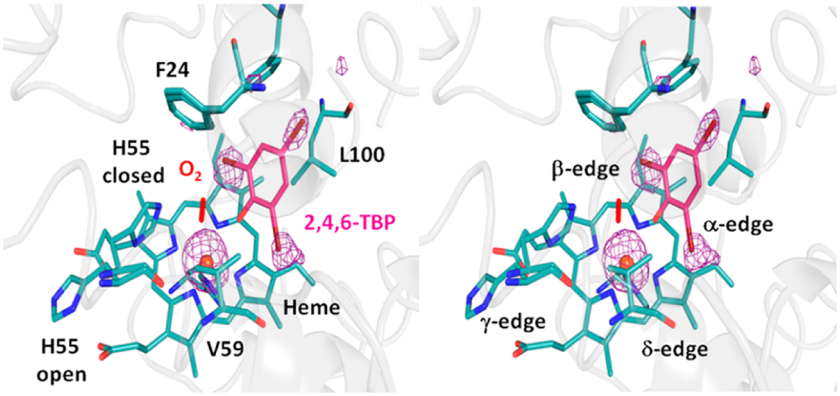

Figure 1. Stereoview of the distal side of the heme pocket of DHP A (PDB entry 4HF6), showing the position occupied by the substrate, 2,4,6-TBP (magenta), at an internal binding site in back of the distal pocket. The heme is shown, as are amino acid residues L100, F24, V59, and H55 in two conformations (open and closed). The substrate location was determined with the help of the anomalous difference electron density map contoured at a 3σ electron density level constructed from the SAD data set at the Kα electron transition energy for Br ($\lambda \sim 0.92$ Å Br edge) relative to Fe. Anomalous density is shown in the figure for the three Br atoms and the heme Fe.

Scheme 2. Two Models for Substrate Inhibition

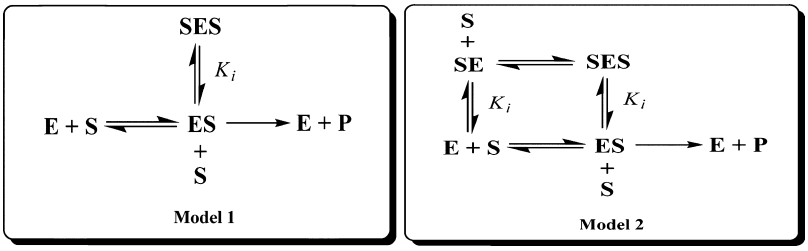

substrate soaking crystals of DHP A in mixed solvent systems following established protocols.[25−27]

Because 2,4,6-TBP has such a low solubility in water, we employed a known method of soaking protein crystals in mixtures of 10−20% organic cosolvents in this study to soak preformed crystals of DHP A in solutions containing the substrate.[25−27] Herein, we report the observation of electron density from the substrate in X-ray crystal structures derived from the cosolvents dimethyl sulfoxide (DMSO), methanol (MeOH), and 2-propanol (2-PrOH). Instead of the anticipated external binding site near the heme β-, γ-, or δ-edge, the X-ray crystal structures revealed a well-defined internal binding site for 2,4,6-TBP above the heme α-edge. We conclude that the substrate binds above the α-edge of the heme based on anomalous diffraction of the Br atoms, detected with synchrotron radiation in the vicinity of the Br absorption edge. This method is strongly supported by the observation of heme Fe X-ray absorption, which serves as a standard for quantification of the occupancy and a reference for the positioning of the substrate in the anomalous density of the Br atoms. These findings require reconsideration of the model for two-site inhibition reported previously.[13,14] Moreover, the observation of two distinct internal binding sites (both an inhibitor and a substrate site) in DHP A further expands the mechanistic possibilities of the globin protein family.

Kinetic studies conducted to determine the functional role of the internal binding site revealed substrate inhibition, in which the activity of the enzyme reaches a maximum at a particular substrate concentration and then declines as the substrate concentration is increased further. This phenomenon is known as substrate inhibition. Substrate inhibition may be attributed to multiple substrate binding sites,[28] an allosteric effect upon substrate binding,[29] or slow enzymatic conformational relaxation.[30] Most of the substrate inhibition models are based on the steady state assumption; thus, the rate equations can always be written in a variant form of the Michealis−Menten equation. Two possible models that involve binding of two substrates to the enzyme are shown in Scheme 2.

The models indicate possible ordering of substrate, S, binding in two different sites, which are indicated by SE or ES. If substrates are bound in both sites, then the species is named SES. Inhibition occurs when a second substrate molecule S binds to the ES complex in a site different from that to which the first molecule bound. We consider both possibilities for the internal site; it could be either an inhibitor or a substrate binding site. It is likely that the significance of the internal site will become evident when the full range of ecological toxins confronted by *A. ornata* is investigated.

MATERIALS AND METHODS

Protein Purification and Crystal Growth. Wild-type DHP A was expressed in Rosetta(DE3) cells; expression was induced with 0.4 mM IPTG, and cells were harvested after growing overnight at room temperature. The expressed protein was purified as previously reported.[7,31−33] Briefly, the protein was purified by ammonium sulfate precipitation, followed by ion exchange SP FF (GE Healthcare) chromatography, and subsequently by gel exclusion chromatography on Sephacryl S-100. The purified protein was concentrated to 10 mg/mL in 20 mM cacodylate buffer (pH 6.5) and crystallized by hanging drop vapor diffusion at 4 °C. The reservoir solution contained 0.2 M $(NH_4)_2SO_4$ and 32% (w/v) PEG 4000.[7,31−33] To obtain crystals of DHP A complexed with substrate, the crystals were further soaked for 24 h in a saturated solution of 2,4,6-TBP

dx.doi.org/10.1021/bi301307f | *Biochemistry* XXXX, XXX, XXX−XXX

Table 1. Data Collection and Refinement Statistics for the 2,4,6-Tribromophenol Structure in Solvents[a]

	10% DMSO	10% 2-propanol	20% methanol
PDB entry	4FH6	4ILZ	4FH7
space group	$P2_12_12_1$	$P2_12_12_1$	$P2_12_12_1$
unit cell parameters			
a (Å)	57.63	57.59	57.57
b (Å)	67.25	67.18	67.27
c (Å)	69.00	68.91	68.94
	Data Collection[b]		
temperature (K)	100	100	100
wavelength (Å)	0.91339	0.91339	0.91339
resolution (Å)	35.0−1.44 (1.48−1.44)	35.0−1.91 (1.96−1.91)	35.0−1.74 (1.78−1.74)
no. of unique reflections	46300 (3375)	20174 (1441)	26513 (1915)
completeness (%)	98.88 (98.61)	99.52 (97.69)	99.71 (98.38)
R_{merge} (%)	8.9 (41.3)	15.6 (31.3)	11.6 (42.8)
$I/\sigma I$	11.9 (2.69)	2.2 (4.2)	5.1 (4.0)
redundancy	3.6 (3.5)	3.7 (3.8)	3.7 (3.9)
	Refinement		
R_{work} (%)[c]	20.1	24.0	22.6
R_{free} (%)[d]	23.3	28.7	27.3
no. of atoms			
protein	2945	2841	3027
water	229	187	241
rmsd[e] from ideal			
bond lengths (Å)	0.008	0.008	0.007
bond angles (deg)	2.50	2.415	2.315
Ramachandran plot (%)[f]			
most favored	94.4	94.4	93.3
allowed	5.6	5.6	6.7
generously allowed			

[a]Crystals were soaked in 250 mM 2,4,6-tribromophenol at the indicated solvent concentration. [b]Values in parentheses are for the highest-resolution shell. [c]$R_{merge} = \sum_h\sum_i[|I_i(h) - \langle I(h)\rangle|/\sum_h\sum_i I(h)] \times 100\%$, where I_i is the *i*th measurement and $\langle I(h)\rangle$ the weighted mean of all measurements of $I(h)$. [d]$R_{work} = \sum|F_o - F_c|/\sum F_o \times 100\%$, where F_o is the observed and F_c the calculated structure factor. [e]R_{free} is the *R* factor for the subset (5%) of reflections selected before, and not included in, the refinement. [f]The rmsd is the root-mean-square deviation. [g]Calculated using PROCHECK.

dissolved in 10 or 20% cosolvent, which consisted of DMSO, 2-PrOH, or MeOH at 4 °C. For data collection, they were flash-cooled in liquid nitrogen after being briefly cryoprotected in a solution consisting of 0.2 M $(NH_4)_2SO_4$ and 35% PEG 4000 supplemented with 15% PEG 400 as a cryoprotectant.

As previously reported,[7,31−33] the protein crystallized in the primitive orthorhombic $P2_12_12_1$ space group with two polypeptide chains per asymmetric unit and the following unit cell dimensions: a = 57.6 Å, b = 67.2 Å, and c = 69 Å.

Data Collection, Processing, and Refinement. Data sets were collected at 100 K on the SER-CAT 22-BM beamline at the Advanced Photon Source synchrotron facility (Argonne National Laboratory, Argonne, IL). Data sets were collected near the Br absorption edge (λ = 0.91942 Å), chosen for the collection of the data in a single-wavelength anomalous dispersion mode to correctly orient the Br atoms of substrate 2,4,6-TBP in its electron density, generated by constructing anomalous difference electron density maps.

A total of 240 images were collected in the inverse-beam mode, using a 1° oscillation range. The diffraction data sets were processed using DENZO and SCALEPACK from the HKL2000 package.[34] The structures were determined by molecular replacement with Phaser,[35] using 1.62 Å resolution structures of metaquo DHP A determined at 100 K (PDB entry 2QFK) as a starting model. The subsequent refinement steps were conducted with the CCP4 suite of programs (Collaborative Computational Project, 1994). To help in the identification of the substrate binding site, anomalous difference Fourier electron density maps were calculated with phases from the final refined model of the 2,4,6-tribromophenol-derivatized structure and $|F^+| - |F^-|$ coefficients, corresponding to wavelength-dependent Bijvoet differences. The Br atoms were placed into the electron density relative to heme iron, which also exhibits an anomalous signal at the X-ray wavelength used for this study. The Fe K absorption edge is observed at 1.74 Å, which is in the range to produce significant anomalous diffraction at the wavelength used for structure determination. Therefore, the observed anomalous diffraction consists of four peaks (one from Fe and three from Br). This fortuitous observation was used to calibrate the occupancy of the 2,4,6-TBP substrate in the internal binding site.

Final models were obtained by iterative cycles of model building in COOT[36] using $2F_o - F_c$ (contoured at 1σ) and $F_o - F_c$ electron density maps (contoured at 3σ) and model refinement using Refmac5[37] in the CCP4 suite of programs (Collaborative Computational Project, 1994). The data set for the crystal soaked with substrate in 10% DMSO diffracted to a resolution of 1.44 Å and refined with the R and R_{free} values of 20.1 and 23.3%, respectively (PDB entry 4FH6). The data set for the crystal soaked in 10% 2-PrOH containing the substrate diffracted to 1.91 Å and refined to R and R_{free} values of 24.0 and 28.7%, respectively (PDB entry 4ILZ). Finally, the crystal soaked in substrate dissolved in 20% MeOH diffracted to a resolution of 1.74 Å and refined to R and R_{free} values of 22.6

dx.doi.org/10.1021/bi301307f | Biochemistry XXXX, XXX, XXX−XXX

and 27.3%, respectively (PDB entry 4FH6). All of the structures had the substrate bound in subunit A, and only the structure with DMSO used as the solvent for the substrate soak contained the substrate in subunit B, as well. The occupancy of the substrate under all the soaking conditions was rather low, around 10%, because of the low substrate solubility in aqueous solutions, and the position of the substrate could be determined only after constructing anomalous difference maps for the data collected at the Br absorption edge. The structures were deposited in the Research Collaboratory for Structural Bioinformatics (RCSB) Protein Data Bank. Final data collection and refinement statistics are summarized in Table 1. Figures showing the X-ray crystal structure were created with PyMOL.[38]

Resonance Raman Spectroscopy. DHP A samples at a final protein concentration of 100 μM were prepared in 100 mM KPB (pH 7.0) with 0, 10, and 20% (v/v) MeOH. Samples were placed in 5 mm NMR tubes and spun with an air piston spinning sample holder (Princeton Photonics, model Raman 101). Resonance Raman spectra were obtained by excitation of the Soret band at 406 nm by using a Coherent Mira 900 Ti:sapphire laser that is tunable generating a 700−1000 nm beam, which was then sent through the Coherent 5-050 doubler to generate the working range of 400−430 nm light for Soret band excitation. The Ti:sapphire laser was powered by the Coherent Verdi 10 frequency-doubled diode-pumped Nd:vanadate laser that generated 10 W of 532 nm light. The frequency-doubled beam was collimated and cylindrically focused to a vertical line of ~5 mm and typically 45−60 mW at the sample. Raman scattered light was collected by the Spex 1877 Triplemate monochromator (2400 grooves/mm final stage grating) and was detected by a liquid N_2-cooled CCD camera (ISA Spex, model CCD-3000). Spectra were measured at room temperature for 40 acquisitions with a total exposure time of 1200 s. The spectra were calibrated using a standard spectrum of toluene, carbon tetrachloride, and cyclohexane.

Kinetic Measurement of Two Related Substrates, 2,4,6-TCP and 2,4,6-TBP. Solutions of each potential substrate in 100 mM KPB (pH 7.0) (KPB) with 10% (v/v) DMSO, 2-PrOH, and MeOH were prepared, as well as a solution containing 20% (v/v) MeOH in KPB. The concentration of 2,4,6-TBP was determined by monitoring the maximal absorbance at 318 nm for KPB with 10% DMSO, 317 nm for KPB with 10% 2-PrOH, and 316 nm for both KPB and MeOH mixtures. Because all solutions are either pure KPB or mixed solvents in KPB, we will omit the label KPB in our description of the buffers with cosolvents. The extinction coefficient (ε) used to calculate the concentrations of 2,4,6-TBP was 4640 M^{-1} cm^{-1}, which was determined in H_2O at 316 nm. The concentration of 2,4,6-TCP was determined by monitoring the maximal absorbance at 312 nm for solutions in KPB and in 10% MeOH based on the extinction coefficient (ε) for 2,4,6-TCP of 3752 M^{-1} cm^{-1} at 312 nm in H_2O. The DHP A stock solution (120 μM) was prepared in KPB. An H_2O_2 stock solution (7.2 mM) was freshly prepared prior to each kinetic assay in KPB, with 10% by volume for each of the cosolvents.

The kinetic assays were conducted in KPB with each of the cosolvents using an Agilent 8453 UV−visible spectrophotometer equipped with a Peltier temperature controller. The catalytic reactions were conducted in a 0.4 cm path length cuvette from Starna Cells, Inc., with a total volume of 1200 μL. The ferric DHP A final concentration $[E]_0$ in each sample was 2.4 μM. Substrate 2,4,6-TXP (X = Br or Cl) final concentrations ranged from 100 to 1200 μM. Ferric DHP A and substrate 2,4,6-TXP were first mixed in the optical cuvette, which was placed in the thermal cell to allow them to reach thermal equilibrium (3 min incubation). All the kinetic assays were conducted at 25 °C. Subsequently, an aliquot of the H_2O_2 stock solution was added to the cuvette to yield a final concentration of 1200 μM, which initiated the reaction. The kinetic data were obtained by monitoring the absorbance at wavelengths of 272 nm for 2,4,6-TBP and 273 nm for 2,4,6-TCP, which correspond to the absorbance peaks of the 2,6-dibromoquinone (DBQ) and 2,6-dichloroquinone (DCQ) products with extinction coefficients of 14000 M^{-1} cm^{-1} (ε_{272}) and 13200 M^{-1} cm^{-1} (ε_{273}), respectively. Data collection was initiated 1.4 s after the addition of H_2O_2. The initial rate was calculated on the basis of the linear fit of the first 10 s of data collection in the photodiode array spectrophotometer. The data obtained as a function of either 2,4,6-TCP or 2,4,6-TBP concentration were then fit to the Michaelis−Menten equation and proposed substrate inhibition model using Igor Pro version 6.04.

Kinetic Analysis of the Models for Substrate Inhibition. Models 1 and 2, shown in Scheme 2, are based on the idea that substrate can bind as an uncompetitive and competitive inhibitor, respectively. The initial rate equation for model 1 is

$$V_0 = \frac{V_{max}[S]}{K_m + [S] + \frac{[S]^2}{K_i}} \quad (1)$$

For model 2, the initial rate equation becomes

$$V_0 = \frac{V_{max}[S]}{K_m + \frac{K_m[S]}{K_i} + [S] + \frac{[S]^2}{K_i}} \quad (2)$$

However, in cases where the substrate binds in the protein interior, the diffusion rate of the substrate may become an important aspect of the kinetic scheme, which can further enhance substrate inhibition.[39] To incorporate internal diffusion into the rate equations, we start with Fick's first law of diffusion

$$J = -D\frac{dc}{dx} = sc \quad (3)$$

where D is the diffusion coefficient, c is the concentration, and s is the drift speed.

The flux J is related to the rate when multiplied by area A and divided by unit volume V, so that

$$v = \frac{JA}{V} = -\frac{DA}{V}\frac{dc}{dx} \quad (4)$$

Assuming that there is a substrate concentration gradient between the exterior and interior of the protein, we can express that gradient as

$$\frac{dc}{dx} = \frac{[S] - [S_0]}{\delta} \quad (5)$$

where effective distance δ is very small, because it comprises the distance from the solvent to the interior of the protein. The expression for the diffusion rate v is

dx.doi.org/10.1021/bi301307f | Biochemistry XXXX, XXX, XXX−XXX

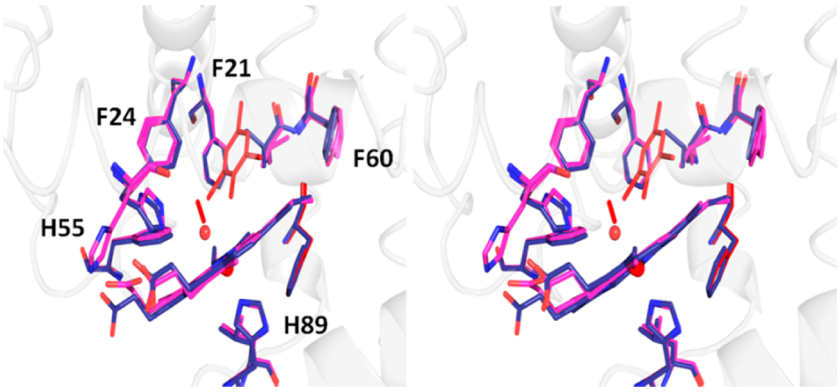

Figure 2. Stereoview of the heme distal pocket. Overlay of the 2,4,6-TBP-bound DHP structure (PDB entry 4HF6) and the metaquo structure (PDB entry 2QFK) depicted as pink and blue sticks, respectively. Water from the metaquo structure bound to heme iron and molecular oxygen and 2,4,6-TBP substrate bound in the distal pocket of the 4FH6 structure are colored red.

$$v = \frac{JA}{V} = -\frac{DA}{V}\frac{dc}{dx} = -\frac{DA}{V\delta}([S] - [S_0]) = k_s([S_0] - [S]) \quad (6)$$

where $[S_0]$ is the bulk solution substrate concentration, $[S]$ is the microenvironment substrate concentration, and k_s is the transport coefficient. If substrate diffusion is the rate-limiting step and the catalytic reaction takes place in the distal pocket where the microenvironment substrate concentration equals $[S]$, the diffusion rate v should be equal to the initial rate of the enzymatic reaction once steady state has been achieved.

$$k_s([S_0] - [S]) = \frac{V_{max}[S]}{K_m + [S] + \frac{[S]^2}{K_i}} \quad (7)$$

Here we used eq 1 based on model 1 for the expression of the initial rate. The resulting third-order equation can be solved analytically and coded for nonlinear least-squares fitting as described in the Supporting Information. The diffusion model has a physical justification, described above, but it was also a necessary addition to fit the kinetic data because neither eq 1 nor eq 2 alone was adequate for nonlinear least-squares fitting of the observed data.

RESULTS

The position of the native substrate, 2,4,6-TBP, in the interior of DHP A is shown in Figure 1 based on PDB entry 4FH6 (see Table 1). Mother liquor containing 20% MeOH was used to soak the substrate 2,4,6-TBP into the crystal. The orientation of the substrate was determined on the basis of the anomalous diffraction density of the three Br atoms in relation to that of the heme Fe atom. An additional figure showing the density from the 4FH6 X-ray crystal structure obtained using 10% DMSO is presented in Figure S1 of the Supporting Information. For all three solvents used to soak in the substrate (PDB entries 4FH6, 4ILZ, and 4FH7), the overall structural parameters of the DHP A protein are similar to those of the published metaquo DHP A X-ray crystal structure (PDB entry 2QFK). An overlay of the two structures in the vicinity of the heme is shown in Figure 2.

The most significant observation in the data arises from the anomalous scattering to a resolution of 2.5 Å arising from both Br and Fe. It is fortunate that anomalous scattering from both Br and Fe can be observed at the same diffraction wavelength (λ) of 0.91942 Å.[40] While anomalous scattering is most often used to determine phases,[41] we were able to estimate the occupancy of Br on the basis of the comparison to the anomalous signal of Fe by comparing their known anomalous scattering factors.[42] At the wavelength of the Br anomalous edge, Br has an anomalous scattering factor (f'') of 3.8 e (e = electrons), and the Fe anomalous scattering factor f'' equals 1.39 e at the wavelength of the Br K absorption edge of 0.922 Å. The anomalous scattering cross sections for Fe and Br are shown in Figures S4 and S5 of the Supporting Information, respectively. In the DMSO structure, the strongest Br and the Fe have peaks at the 7.1σ and 23σ levels corresponding to 0.09 and 0.29 electron/Å^3, respectively. Clearly, the Fe signal is much stronger than the Br signal in all of our structures. Because we know that Fe has an occupancy of 1.0, we can obtain a calibration for Br scattering. Therefore, the Fe signal can be used to normalize the electron density of the three Br atoms and to quantify the occupancy of 2,4,6-TBP. From the anomalous scattering factor of 1.39 for the Fe atom, we obtain a normalization of 16.6σ/f'' corresponding to an occupancy of 1.0. The Br atoms in the DMSO structure have a σ/f'' (7.1/3.8) of 1.86, which is approximately 10% as large as the Fe signal. Consequently, we estimate the occupancy of 2,4,6-TBP to be ~0.1.

The density of the anomalous diffraction due to Br shown in Figure 1 at the 3σ level matches perfectly the position of the three Br atoms in 2,4,6-TBP, indicating that the 2,4,6-TBP substrate resides at a site adjacent to L100 deep inside DHP A and is oriented such that its hydroxyl group is positioned within hydrogen bonding distance of a heme Fe-bound O_2 molecule. This orientation obtained for all three structures (PDB entries 4FH6, 4ILZ, and 4FH7) is uniquely defined by the electron density attributable to the three Br atoms by anomalous diffraction. The distances from the substrate to neighboring amino acids, I20, F21, F24, V59, F60, and M63, are listed in Table S1 of the Supporting Information. The substrate encompasses the Xe binding site, which was characterized previously in DHP A;[43] however, unlike the inhibitor 4-BP, none of the bromine atoms are located in the Xe1 binding site.

The fact that a relatively large molecule can be accommodated deep inside the globin above the α-edge of the heme (Figure 1) is distinct from the previous observation that the inhibitor, 4-BP, also has a binding site in the distal pocket located immediately above the heme iron.[13,44,45] An overlay of the binding sites of inhibitor 4-BP and substrate 2,4,6-TBP is shown in Figure 3. A view of substrate and

dx.doi.org/10.1021/bi301307f | Biochemistry XXXX, XXX, XXX–XXX

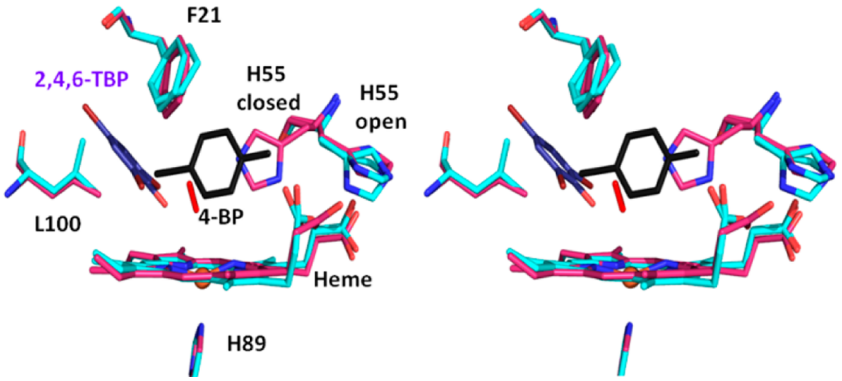

Figure 3. Stereoview of an overlay of the binding site of 2,4,6-TBP (substrate colored purple) and 4-BP (inhibitor colored black) in the distal pocket. The cyan structure is DHP A, which corresponds to the 4-BP inhibitor-bound structure (PDB entry 3LB2), and the purple structure corresponds to the substrate-bound structure (PDB entry 4FH6).

inhibitor separately is given in panels A and B of Figure S2 of the Supporting Information. Aside from the location of the respective binding sites, the only major difference between the inhibitor- and substrate-bound X-ray crystal structures arises from the fact that heme Fe is reduced and O_2 is bound in the substrate-bound structure. For example, the 4FH7 structure is almost 100% in the oxy form (see Table 2). The inhibitor-bound X-ray structure (PDB entry 3LB2) lacks a sixth heme Fe ligand and thus is 5cHS. We have previously discussed the relative susceptibility of DHP A to reduction by the X-ray beam in synchrotron experiments.[33] Ferric DHP A has a high redox potential[46] and appears to be readily reduced to the ferrous state even after a brief exposure to synchrotron radiation.[32,47] Because O_2 is not excluded under the conditions used in these experiments, it can bind to ferrous Fe to make the oxy-DHP A adduct. The fact that the hydroxyl group of 2,4,6-TBP is positioned within hydrogen bonding distance of the O atom bound to the heme Fe also suggests a possible mechanistic aspect of substrate binding. The bound substrate does not appear to compete with the separate binding of a ligand to the heme Fe. Thus, 2,4,6-TBP binding in this site does not necessarily lead to inhibition, simply based on structural considerations. However, the kinetic data show that substrate inhibition occurs at a sufficiently high concentration.

Table 2. Substrate Structural Parameters in the Distal Heme Pocket of Subunit A

	2,4,6-tribromophenol-bound DHP A (4FH7)	metaquo form of DHP A (2QFK)[a]
Fe–His89 $N^{\varepsilon 2}$ (Å)	2.0	2.1
Fe–His55 $N^{\varepsilon 2}$ (Å)[b]	5.5	4.8
Fe–OH(TBP) (Å)[c]	3.73	–
Fe–O (Å)[d]	2.95 (O_2)	2.2 (H_2O)
OH(TBP)–O_2		
O1 (Å)[e]	2.55	–
O2 (Å)[e]	2.66	–
Fe–pyrrole N plane (Å)	0.22	0.04
Fe–substrate bend angle (deg)	166.99	–
Fe–substrate tilt angle (deg)[f]	42.8	–
Fe–O_2 bend angle (deg)	167.5	–
Fe–O_2 tilt angle (deg)[f]	13.8	–

[a]From ref 32. [b]Distance to the His55 conformer located inside the distal cavity. [c]The Fe–OH(TBP) distance is the distance between the iron and hydroxyl oxygen of the phenyl moiety of the substrate. [d]The Fe–O distance refers to the distance between the iron and first oxygen atom of the molecular oxygen bound in the distal cavity in the substrate-bound structure or between the iron and water oxygen in the metaquo structure. [e]Distances between the substrate hydroxyl oxygen and the two oxygen atoms of the molecular oxygen in the distal pocket. [f]The tilt angle is the angle between the heme perpendicular and the Fe–O bond.[63]

Because of the limited solubility of 2,4,6-TBP in an aqueous solution, the nonaqueous solvents DMSO, 2-PrOH, and MeOH were used to increase its concentration in enzymatic assays. The three cosolvents were mixed with KPB to prepare aqueous solutions of 2,4,6-TBP at sufficient concentrations to permit comparison with 2,4,6-TCP in kinetic assays. Figure S6 of the Supporting Information shows that the solvents did not have a major effect on the absorption spectra of the ferric form of DHP A, with the exception of DMSO, which caused substantial shifts in the Soret band to longer wavelengths at DHP A concentrations of <10 μM (Figure S6 of the Supporting Information). The resonance Raman spectrum shown in Figure 7 indicates that the heme structure is not significantly altered in 10 or 20% methanol. However, there is an increase in the magnitude of the six-coordinate high spin (6cHS) component relative to that of the five-coordinate high spin (5cHS) component. The increase in the 6cHS component provides an explanation for the reduction in the initial rate observed in the kinetic studies as the percentage of MeOH increases. The 6cHS component in aqueous solutions of ferric DHP A is the metaquo form, i.e., Fe(III)–OH_2. H_2O ligated to the heme Fe tends to inhibit the binding of H_2O_2 and thus reduces the catalytic rate in agreement with the observations in Figures 4–6. DMSO may further strengthen the tendency of H_2O to partition into the distal pocket but may also interact with the heme Fe itself. Either of these possibilities would explain the near absence of any kinetic turnover in 10% DMSO solutions, despite the apparent structural integrity of the DHP A protein crystals soaked in 10% DMSO. As shown in Figure 4, DHP A enzymatic activity was reduced 100-fold in a 10% DMSO solution. The reduction in activity in 10% 2-PrOH did not have such a drastic effect; it still caused a <50% reduction in enzymatic activity as can be seen in Figure 4. The X-ray crystal structure and absorption spectra of DHP A strongly suggest that the structure and heme environment were not affected in these solutions; rather, the kinetic effects result in changes in

dx.doi.org/10.1021/bi301307f | *Biochemistry* XXXX, XXX, XXX–XXX

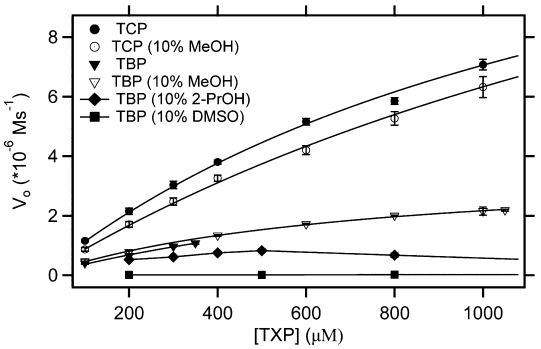

Figure 4. Single-wavelength kinetics of DHP-catalyzed 2,4,6-TXP (X = Br or Cl) oxidation as a function of substrate concentration and enzymatic reaction initial rate in KPB with or without 10% MeOH. The assay conditions were 2.4 μM ferric DHP A and 1200 μM H_2O_2.

heme ligation in the ferric resting state. Our kinetic model applied to the data suggests that the further reductions in rate at high substrate concentrations may be due to substrate inhibition.

The effect of MeOH cosolvent on enzyme kinetics is relatively small. Experiments using substrate 2,4,6-TCP in KPB with 10% MeOH cosolvent show that the catalytic efficiency, k_{cat}/K_m, is reduced by ~25% relative to that in KPB buffer alone (Table 3). This effect may be mainly due to the lowered surface

Table 3. Kinetic Parameters from Curve Fitting to the Michaelis–Menten Equation

	k_{cat} (s^{-1})	K_m (mM)	k_{cat}/K_m (s^{-1} mM^{-1})
2,4,6-TCP	7.07 ± 0.48	1.40 ± 0.15	5.05 ± 0.08
2,4,6-TCP (10% MeOH)	8.59 ± 0.73	2.26 ± 0.27	3.80 ± 0.08
2,4,6-TBP	1.92 ± 0.84	1.15 ± 0.63	1.67 ± 0.82
2,4,6-TBP (10% MeOH)	1.55 ± 0.05	0.71 ± 0.05	2.18 ± 0.01

binding affinity of 2,4,6-TCP, because k_{cat} is actually increased in 10% MeOH (Table 3). These experiments show that MeOH is a feasible cosolvent for kinetic studies of 2,4,6-TBP, which increases the concentration range above the limit of solubility of 270 μM 2,4,6-TBP in KPB.[10,19,48] The kinetic data in Figure 4 show that 2,4,6-TBP follows Michealis–Menten kinetics in a 10% MeOH/KPB mixture in the concentration range from 0 to 1400 μM, so that the rate parameters can be compared with those of 2,4,6-TCP for the first time. The catalytic rate, k_{cat}, is ~6 times slower for 2,4,6-TBP; however, this is compensated by a greater enzymatic on rate observed in the value of K_m, which is ~3 times smaller for 2,4,6-TBP. We also determined the activation energy for 2,4,6-TBP compared to that of 2,4,6-TCP using a combination of Arrhenius and Michaelis–Menten analyses published previously. The result is that there is only a small difference, with the values being 39.6 kJ/mol for 2,4,6-TCP and 45.5 kJ/mol for 2,4,6-TBP (Figure S7 of the Supporting Information).

The X-ray crystal structure 4FH7 was obtained in 20% MeOH, which prompts a comparison of the kinetics at the highest possible substrate concentration. Figure 5 shows a comparison of the kinetics of turnover of 2,4,6-TBP extended to the highest possible concentrations at 10, 15, and 20% MeOH in KPB. The limits of 2,4,6-TBP solubility in 10, 15, and 20% MeOH are ~1200, 1800, and 2500 μM, respectively.

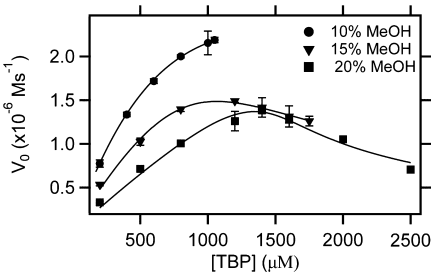

Figure 5. Single-wavelength kinetics of DHP-catalyzed 2,4,6-TBP oxidation as a function of substrate concentration and enzymatic reaction initial rate in KPB with 10, 15, and 20% MeOH. The assay conditions were 2.4 μM ferric DHP A and 1200 μM H_2O_2.

While 10% MeOH shows a behavior analogous to the kinetics observed in pure KPB, the turnover frequency in 15 and 20% MeOH is reduced. Moreover, Figure 5 shows that a maximum in the rate is reached at ~1400 μM 2,4,6-TBP and that the rate decreases above this concentration in both 15 and 20% MeOH. Attempts to fit the kinetics in 15 and 20% MeOH using the modified Michaelis–Menten kinetic equations given by models 1 and 2 were not successful. Instead, the modified Michaelis–Menten diffusion model discussed in the introductory section (and further elucidated in the Supporting Information) was applied to fit the data. The fit shown in Figure 5 accounts for the maximum in the kinetic rate. Moreover, this modified kinetic model can also explain the maximum in the rate at 500 μM observed in 10% 2-PrOH solvent, which is shown in Figure S8 of the Supporting Information. Figure 6 shows the kinetics

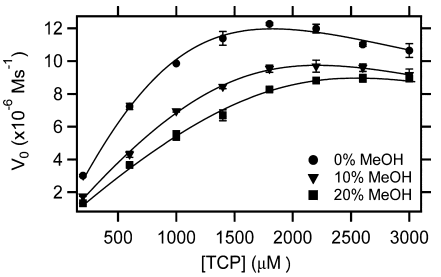

Figure 6. Single-wavelength kinetics of DHP-catalyzed 2,4,6-TCP oxidation as a function of substrate concentration and enzymatic reaction initial rate in KPB with 0, 10, and 20% MeOH. The assay conditions were 2.4 μM ferric DHP A and 1200 μM H_2O_2.

as a function of 2,4,6-TCP concentration up to a maximal concentration of 2500 μM. As observed for the native substrate, 2,4,6-TBP, the turnover frequency of 2,4,6-TCP reaches a maximum at ~1800 and ~2000 μM in KBP and 10% MeOH, respectively. The trend of a decreasing rate with an increasing percentage of MeOH is observed for 2,4,6-TCP, just as reported above for 2,4,6-TBP.

The Soret band resonance Raman spectrum was obtained in KBP as well as 10 and 20% MeOH/KBP mixtures. The spectral region shown in Figure 7 is the core size marker region that includes modes ν_2, ν_3, and ν_{10}, among others. These modes are sensitive to the spin and coordination state of the heme. We have previously discussed the fact that DHP has a 60:40 mixture of six-coordinate high-spin (6cHS) and five-coordinate high-spin (5cHS) populations at room temperature. This observation appears to be correlated with the room-temperature X-ray crystal structure showing that the distal histidine,

dx.doi.org/10.1021/bi301307f | Biochemistry XXXX, XXX, XXX–XXX

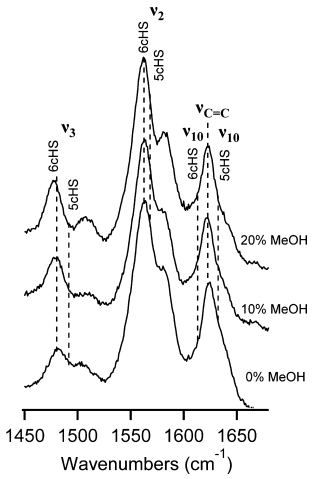

Figure 7. Resonance Raman spectra of the core size maker band region for DHP A in 100 mM KPB (pH 7.0), DHP A in 100 mM KPB (pH 7.0) with 10% MeOH, and DHP A in 100 mM KPB (pH 7.0) with 20% MeOH. The final concentration of DHP A was 100 μM. The excitation wavelength was 406 nm, the resolution 0.9 cm^{-1}, and the acquisition time 1200 s.

H55, is in the distal pocket (internal) and solvent-exposed (external) conformations in the same ratio. Thus, our model has been that the internal conformation of H55 stabilizes a heme Fe-bound H_2O molecule, which with H55 in the external conformation leads to a 5cHS heme with no H_2O ligand. Figure 7 shows that the 6cHS population increases relative to the 5cHS component as the MeOH concentration increases. However, aside from the subtle change in the coordination of the heme Fe atom, there are no major changes in the resonance Raman spectrum.

DISCUSSION

Both the X-ray crystal structures of 2,4,6-TBP soaked into crystals of DHP A (Figures 1−3) and the enzyme kinetics (Figures 4−6 and Table 4) strongly suggest that the native substrate can bind deep inside the protein above the heme α-edge. However, the kinetic data also suggest that at low concentrations, the binding and activation of the native substrate 2,4,6-TBP are quite similar to those of the model substrate 2,4,6-TCP that has been used in most studies of DHP A and B. The available data from NMR, EPR, and resonance Raman spectroscopy corroborate the hypothesis that the binding site of the substrate analogue 2,4,6-TCP is near the heme edge (either β- or δ-edge) on the protein exterior.[11,13,14,22,49−51] Therefore, we initially expected to find a binding site for 2,4,6-TBP on the protein exterior as well. In fact, 2,4,6-TBP has a pK_a lower than that of 2,4,6-TCP, which means that an even greater fraction of the substrate 2,4,6-TBP is negatively charged at physiological pH. Therefore, the lower rate of 2,4,6-TBP relative to that of 2,4,6-TCP may be attributed to the pK_a difference, which is consistent with the charge repulsion between DHP and the 2,4,6-TCP established previously by ionic strength and mutational studies.[18] However, in this work, the kinetic data obtained at higher 2,4,6-TBP concentrations (>1400 μM) indicate that there may be an additional substrate binding site, which at acts as an inhibitor. The most plausible model is that there is one external (SE) and one internal binding site (ES), which connects the observed data to the models in Scheme 2. However, the simple models using the only solution of the rate equations by the steady state approximation failed to fit the kinetic data in Figures 5 and 6. The model that fits the data is consistent with substrate activation in the internal site with a requirement for diffusion into the protein interior. The origin of inhibition is not entirely clear from the structure and is dependent on the structural details of the internal and external sites. This comparison is hampered by the fact that the position of the external site is still not known.

Dichotomy between Internal and External Binding Sites. The dichotomy between internal and external modes of binding has been a pervasive theme in studies of DHP. Initially, the internal site observed in the first published X-ray crystal structure (PDB entry 1EWA) was assumed to be the substrate binding site,[44,45] despite the fact that 4-iodophenol (4-IP), and not the putative substrate 2,4,6-TBP, was observed in that site. An external substrate binding site near the heme β-, γ-, or δ-edge has been hypothesized to explain enzyme kinetic data, obtained using 2,4,6-TCP. Extensive data are consistent with a one-electron oxidation mechanism[11,16,22,52] and competitive inhibition by 4-BP.[13] Structural evidence of an external binding site for 2,4,6-TCP comes from NMR,[49,50] flow EPR,[22] and resonance Raman spectroscopy.[13,51] However, there is also evidence of internal interactions of molecules ranging from imidazole to 2,4,6-TBP in the interior of DHP A, obtained from cryogenic FTIR spectroscopy[12,53] and X-ray crystallography.[44,45] Most recently, we have advanced a two-site competitive inhibition model for 2,4,6-TCP (substrate) and 4-BP (inhibitor). The two-site model is absolutely necessary because 2,4,6-TCP clearly does not bind in the internal site that 4-BP occupies, yet there is strong evidence of competitive inhibition of 2,4,6-TCP by 4-BP.[13] Consideration of the body of data that led to the two-site competition model is warranted to improve our understanding of the possible ramifications of an internal heme α-edge internal binding site in DHP A (Figures 1−3).

Table 4. Kinetic Parameters Obtained from Fitting to the Proposed Model at 298 K

	k_{cat} (s^{-1})	$K_m(K_i)$ (mM)	k_{cat}/K_m (s^{-1} mM^{-1})	μ
		2,4,6-TBP		
10% MeOH	2.87 ± 0.11	1.54 ± 0.37	1.86 ± 0.11	~0
15% MeOH	1.86 ± 0.03	0.72 ± 0.07	2.58 ± 0.01	1.47 ± 0.37
20% MeOH	1.71 ± 0.06	0.51 ± 0.05	3.38 ± 0.04	4.95 ± 0.97
10% 2-PrOH	1.00 ± 0.03	0.30 ± 0.03	3.29 ± 0.03	1.97 ± 0.49
		2,4,6-TCP		
0% MeOH	14.96 ± 0.20	1.49 ± 0.13	10.04 ± 0.01	0.67 ± 0.24
10% MeOH	12.18 ± 0.09	1.53 ± 0.10	7.96 ± 0.01	1.34 ± 0.22
20% MeOH	11.21 ± 0.14	1.63 ± 0.17	6.88 ± 0.01	1.70 ± 0.38

dx.doi.org/10.1021/bi301307f | Biochemistry XXXX, XXX, XXX−XXX

Probes of the Internal Binding Site Based on Diatomic Ligand Dynamics. Since the observation that 4-IP binds in the distal pocket of DHP A,[44,45] there has been a systematic investigation of the effect of molecular binding on the distal cavity of the protein. FTIR spectroscopy at cryogenic temperatures using both the frequency and the temperature-derivative spectroscopy (TDS) of a CO ligand has provided evidence that a number of small molecules, besides 4-IP, can enter the distal pocket.[12,53] TDS reports on the energy barrier for rebinding of a CO ligand photolyzed at low temperatures. In these experiments, as the temperature is gradually increased the CO molecule will recombine with the heme Fe when the thermal energy is sufficient. By measuring the effect on CO rebinding, we determined that many different molecules can bind in the inhibitor binding pocket, immediately above the heme Fe and perpendicular to the plane of the heme (Figure 3). However, systematic comparison of the binding of the series 4-XP (where X = I, Br, Cl, F, or H) in the inhibitor site established that the binding constant of 4-IP is strongest with 4-BP as the second strongest.[9] This is particularly important because 4-BP is present at a ratio of 2:1 with 2,4,6-TBP in benthic ecosystems.[2−5] Molecules with ortho substituents bind less well. For example, 2,4-dichlorophenol (2,4-DCP) binds much more weakly, and 2,4,6-TFP binds even more weakly based on the TDS[12] and NMR.[50] On the basis of the small shifts in the frequency of bound CO at cryogenic temperatures, we concluded that the native substrate 2,4,6-TBP binds extremely weakly or alternatively has a small effect on the binding of CO. FTIR has provided no evidence of internal binding at higher temperatures. However, the X-ray structural data shown in Figure 2 show that that heme-bound CO would not be strongly affected by 2,4,6-TBP binding (because O_2 is able to bind at the same time as 2,4,6-TBP). Consistent with the requirement for a substrate binding site, the heme α-edge binding site does not prevent diatomic ligand binding to the heme Fe (Figures 1−3). This observation is crucial for the hypothesis that the internal site is a substrate binding site because the substrate should not interfere with the binding of cosubstrate H_2O_2. Moreover, the X-ray crystal structure (Figures 1−3) shows that there is no hindrance for the entrance or exit of small molecules (e.g., H_2O_2) through a proposed channel near the distal histidine, H55.

Opposition of Internal and External Sites in the Two-Site Competitive Inhibition Mechanism. More recently, competitive inhibition was observed in DHP A and interpreted to arise from the switching of the conformation of H55 between both internal inhibitor and external substrate binding.[13] In the model of two-site competitive inhibition, it was suggested that substrate binds on the outside and pushes H55 into the interior (closed position) while 4-BP binds on the inside pushing H55 toward the exterior of the distal cavity (open position). Thus, H55 was proposed to act as the mediator between the interior and exterior binding sites. The NMR data show that molecules such as 4-BP affect internal amino acid residues such as F21, F35, K58, and V59, while the binding of 2,4,6-TCP as a model substrate affects none of these internal amino acid residues.[49] Instead, 2,4,6-TCP binding affects H55 slightly. 2,4,6-TCP binding also has a small effect on a few surface amino acid residues, including G1, D121, and R122, and has no explanation at present. These amino acids are near the dimer binding site of DHP A. Although DHP A is a crystallographic dimer, the enzyme is 80% monomeric in solution based on small angle X-ray scattering data.[54] Perhaps this observation explains why the substrate does not bind on the exterior of the protein when soaked into the crystal. If the external or surface binding site for 2,4,6-TBP is coincident with one of the dimer interfaces, which are considered in detail in ref 54, then there would be no possibility of high-affinity binding at low 2,4,6-TBP concentrations.

Resonance Raman spectroscopic evidence complements observations based on X-ray crystallography regarding the interaction of 2,4,6-TCP with DHP A. 4-BP binding results in a displacement of H_2O bound to the heme iron, thus resulting in a change in the frequency of the core size marker mode, ν_3.[13,51] The mode shifts from a frequency corresponding to six-coordinate high-spin (6cHS) to five-coordinate high-spin (5cHS) as 4-BP and other 4-halogen analogues, 4-XP (X = I, Br, Cl, or F), are titrated into the distal pocket binding site. On the other hand, when 2,4,6-TCP is bound to DHP, the heme Fe is in the 6cHS form, and accordingly, there is an opposite coordination change from 5cHS to 6cHS. The coordination change to 6cHS has been interpreted as a result of the displacement of the distal histidine, H55, inward to increase its extent of hydrogen bonding to the heme-bound H_2O molecule.

A Structural Model for a Two-Electron Sequential Peroxidase Mechanism. We turn to the question of whether the internal heme α-edge binding site could permit peroxidase reactivity. The mechanism for an internally bound substrate would necessarily involve two sequential one-electron transfers followed by attack by H_2O as shown in Figure 8A. By contrast,

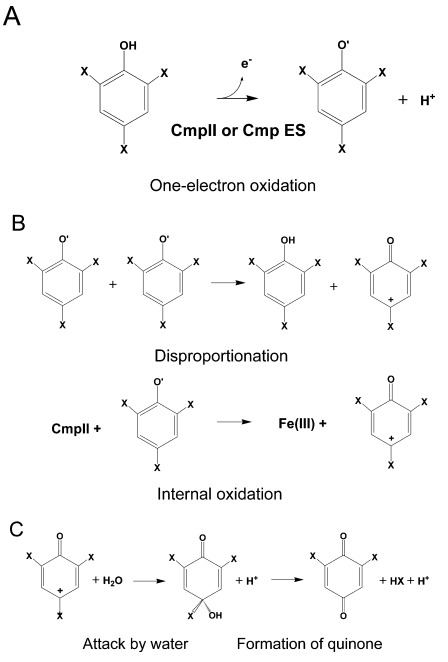

Figure 8. Schematic representation of the mechanisms for oxidation of substrate by DHP A. (A) An initial step involves oxidative electron transfer and loss of H^+ to form a neutral phenoxy radical, 2,4,6-TXPO (X = Cl or Br). (B) Two alternative mechanisms for the oxidation of the 2,4,6-TXPO radical. The disproportionation mechanism occurs in solution and results in formation of 1 equiv of phenoxy cation and 1 equiv of reactant for every 2 equiv of the radical. The internal oxidation mechanism would require the substrate to remain immobilized within the enzyme for a second electron transfer to form the phenoxy cation. (C) Attack of the phenoxy cation by water in the para position leading to displacement of the halogen atom in the form HX and loss of H^+ to give the neutral 2,6-dihaloquinone product.

dx.doi.org/10.1021/bi301307f | *Biochemistry* XXXX, XXX, XXX−XXX

the peroxidase pathway is a one-electron oxidation pathway that normally requires radical intermediates to diffuse into solution and disproportionate to form 1 mol of products and 1 mol of reactants for every two oxidizing equivalents.[9,11,16,22] Previous work has shown that the 2,4,6-TCP phenoxy radical is formed on the first oxidation by compound ES (or by compound II). This is a one-electron oxidation that is observed directly by flow EPR.[22] In the standard peroxidase mechanism, the radical would diffuse into solution and then react by disproportionation as shown in Figure 8B. If 2,4,6-TBP were to be oxidized in the interior of DHP A, then the radical formed by this one-electron oxidation would be trapped inside the protein. Because it is nearly impossible for a radical to diffuse out of the protein, the second electron transfer would be required to take place while the substrate was inside the protein as well. Figure 8C shows that attack by a water molecule on the 2,4,6-trichlorocyclohexa-2,5-dienone cation, which is the final step leading to 2,6-dichloroquinone. The mechanism shown in Figure 8C requires a way for H_2O to attack the para-Br atom in bound 2,4,6-TBP to complete the oxidation process. The fact that there appears to be a H_2O migration channel (Figure 9)

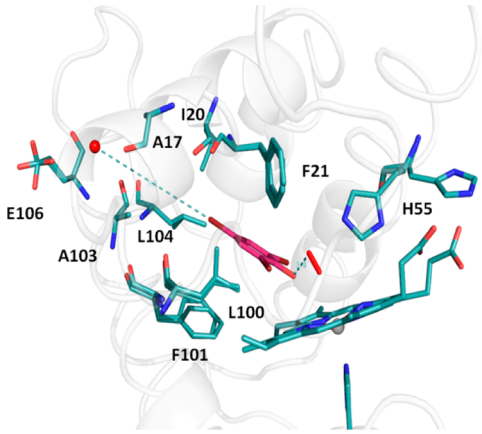

Figure 9. Location of the potential water migration channel required for the DHP A reaction mechanism in PDB entry 4FH6. To aid the removal of Br for 2,4,6-TBP in an internal binding site at position 4 of the substrate, a water molecule must reach the substrate.[24,64] The X-ray crystal structure reveals a channel lined with the carbonyl oxygens from the peptide bonds facing the interior of the channel. The channel leads directly from the surface to the reaction center at position 4 of bound 2,4,6-TBP. The distance of 8.1 Å between the reactive water molecule and the site of oxidation on 2,4,6-TBP is indicated by a dashed line. The residues that may facilitate the translocation of the water molecule are labeled.

that leads directly from the surface of the protein to this Br atom provides a resolution to this problem, suggesting that two sequential one-electron oxidations could occur in the protein, followed by attack by H_2O to complete the mechanism. Subsequently, the product 2,6-DBQ could diffuse out of the protein as indicated by the mechanism in Figure 8C. This mechanistic possibility is included for completeness and because the unusual feature of a second internal binding site in the distal pocket of DHP A raises a number of questions concerning protein function. We suggest that these experiments reveal a new binding site that may have implications for substrates beyond 2,4,6-TBP based on the fact that there are a vast number of brominated alkaloids in benthic ecosystems that may also serve as substrates for DHP in the binding site discovered here.[55]

Relationship to Cytochrome P450 Substrate Binding Sites. The substrate bound at the α-heme edge is tilted at an angle of 46.5° relative to the heme plane and at an angle and proximity to heme Fe that puts the substrate in a position remarkably similar to the position of 1,3,5-trichlorobenzene (TCB) in the structure of the F87W/Y96F/V247L mutant of $P450_{cam}$.[56] The structural comparison is shown in Figure S3 of the Supporting Information, and the parameters are listed in Table S2 of the Supporting Information. This similarity is interesting in that it suggests possible similar modes of binding between the P450 family and DHP. Recent studies using $H_2{}^{18}O$ prove that the O atom in the 2,6-DCQ product comes from H_2O in reactions catalyzed by DHP,[52] in agreement with similar measurements of the same reaction catalyzed by horseradish peroxidase.[24] However, 2,4,6-TXPs are not the only possible substrates for DHP A and B, and it is possible that the internal site can bind other substrate(s). Cytochrome P450 has shown substrate promiscuity, and its oxygenase function takes place primarily in an internal binding pocket above the heme Fe. Correspondingly, substrate inhibition has also been observed for cytochrome P450.[57] Although we can make a structural analogy with cytochrome P450 as shown in Figure S3 and Table S2 of the Supporting Information, the internal binding site of 2,4,6-TBP is not consistent with the rebound mechanism or direct attack by an O atom in compound I because there is no C−H bond at an appropriate position.[58] If the internal site for 2,4,6-TBP is an active site, then the mechanism would necessarily deviate from the standard peroxidase mechanism.

Structural Comparison of Binding Sites in Peroxidases. The binding of a substrate above the α-edge of the heme is novel mode of binding. Figure 10 shows a comparison

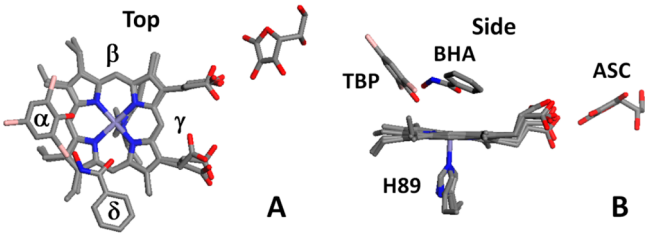

Figure 10. Overlay of the structures of DHP A binding with 2,4,6-TBP (PDB entry 4FH6), HRP binding with BHA (PDB entry 1GX2), and AXP binding with ASC (PDB entry 1OAF). (A) Top view showing the heme edges labeled as α, β, γ, and δ, (B) Side view with the three substrates labeled as 2,4,6-TBP, BHA, and ASC.

of the binding of three different substrates typical of three representative peroxidases. In addition to the three structures reported in Table 1, Figure 10 shows top and side views of an overlay of the binding sites of benzhydroxamic acid (BHA) near the δ-edge of HRP[59] and the binding of ascorbate (ASC) near the γ-edge of AXP[27] (PDB entries 1GX2 and 1OAF, respectively). The binding of substrates near the δ-edge in class III peroxidases such as HRP and lignin peroxidase is well-known.[25] Figure 10 shows that 2,4,6-TBP is bound even closer to the heme Fe than other peroxidase substrates, which permits rapid electron transfer required for a peroxidase mechanism. However, the proximity of 2,4,6-TBP also suggests that direct oxygen atom transfer may be possible in a peroxygenase

dx.doi.org/10.1021/bi301307f | *Biochemistry* XXXX, XXX, XXX−XXX

mechanism for appropriate substrates that bind in this site. These features are unique to DHP.

CONCLUSION

The versatility of DHP is evident from its multifunctional capabilities that currently include oxygen transport,[60] oxidation of brominated phenols by a peroxidase mechanism,[61] and hydrogen sulfide oxidation.[62] The X-ray structure obtained with infused 2,4,6-TBP shows that an internal substrate binding site exists in DHP A that suggests yet another functional possibility, internal oxidation by a two-electron sequential mechanism. The internal substrate binding site is sufficiently large that various environmental toxins could also be accommodated. There are a number of naturally occurring brominated and chlorinated toxins in the marine ecosystem, which suggests that DHP A may have additional detoxification functions that have not yet been discovered.

ASSOCIATED CONTENT

Supporting Information

Figures showing the X-ray crystal structure of PDB entry 4FH6, comparison of substrate and inhibitor binding sites in the distal pocket, comparison of 1,3,5-trichlorobenzene binding to cytochrome $P450_{cam}$ relative to heme iron in DHP A and $P450_{cam}$, anomalous scattering cross sections for Fe and Br, the Soret band shift upon addition of organic solvents, an Arrhenius plot obtained by a linear fit of $\ln(k_{cat}/K_m)$ versus $1/T$, a kinetic study 2,4,6-TBP oxidation catalyzed by DHP in 20% iPrOH buffer, resonance Raman spectra of DHP A in 0, 10, and 20% MeOH/KBP mixtures, and the solution of the modified Michaelis–Menten diffusion equation. This material is available free of charge via the Internet at http://pubs.acs.org.

Accession Codes

Coordinates and structure factors for DHP A in complex with 2,4,6-tribromophenol have been deposited in the Protein Data Bank as entries 4FH6 (10% DMSO), 4FH7 (20% MeOH), and 4ILZ (10% 2-PrOH).

AUTHOR INFORMATION

Corresponding Author

*Phone: (919) 515-8915. Fax: (919) 515-8920. E-mail: stefan_franzen@ncsu.edu.

Author Contributions

J.Z. and V.d.S. contributed equally to this project.

Funding

This project was supported by Army Research Office Grant 57861-LS.

Notes

The authors declare no competing financial interest.

ACKNOWLEDGMENTS

X-ray data were collected at the Southeast Regional Collaborative Access Team (SER-CAT) 22-BM beamline at the Advanced Photon Source. Use of the Advanced Photon Source is supported by the U.S. Department of Energy, Office of Science, Office of Basic Energy Sciences, under Contract W-31-109-Eng-38. We thank Dr. Robert Rose of the North Carolina State University Department of Biochemistry for helpful discussions.

ABBREVIATIONS

DHP A, dehaloperoxidase-hemoglobin A; HRP, horseradish peroxidase; BHA, benzohydroxamic acid; AXP, ascorbate peroxidase; ASC, ascorbate; 4-BP, 4-bromophenol; EPR, electron paramagnetic resonance; 2,6-DBQ, 2,6,-dibromoquinone; 2,6-DCQ, 2,6-dichloroquinone; DMSO, dimethyl sulfoxide; 4-IP, 4-iodophenol; KPB, potassium phosphate buffer; MeOH, methanol; NMR, nuclear magnetic resonance; PDB, Protein Data Bank; 2-PrOH, 2-propanol; TDS, temperature-derivative spectroscopy; 2,4,6-TBP, 2,4,6-tribromophenol; 2,4,6-TCP, 2,4,6-trichlorophenol; 5cHS, five-coordinate high-spin; 6cHS, six-coordinate high-spin.

REFERENCES

(1) Chen, Y. P., Woodin, S. A., Lincoln, D. E., and Lovell, C. R. (1996) An unusual dehalogenating peroxidase from the marine terebellid polychaete *Amphitrite ornata*. *J. Biol. Chem. 271*, 4609–4612.

(2) Fielman, K. T., Woodin, S. A., and Lincoln, D. E. (2001) Polychaete indicator species as a source of natural halogenated organic compounds in marine sediments. *Environ. Toxicol. Chem. 20*, 738–747.

(3) Fielman, K. T., Woodin, S. A., Walla, M. D., and Lincoln, D. E. (1999) Widespread occurrence of natural halogenated organics among temperate marine infauna. *Mar. Ecol.: Prog. Ser. 181*, 1–12.

(4) Lincoln, D. E., Fielman, K. T., Marinelli, R. L., and Woodin, S. A. (2005) Bromophenol accumulation and sediment contamination by the marine annelids *Notomastus lobatus* and *Thelepus crispus*. *Biochem. Syst. Ecol. 33*, 559–570.

(5) Woodin, S. A., Walla, M. D., and Lincoln, D. E. (1987) Occurrence of brominated compounds in soft-bottom benthic organisms. *J. Exp. Mar. Biol. Ecol. 107*, 209–217.

(6) Han, K., Woodin, S. A., Lincoln, D. E., Fielman, K. T., and Ely, B. (2001) *Amphitrite ornata*, a marine worm, contains two dehaloperoxidase genes. *Mar. Biotechnol. 3*, 287–292.

(7) de Serrano, V., D'Antonio, J., Franzen, S., and Ghiladi, R. A. (2010) Structure of dehaloperoxidase B at 1.58 angstrom resolution and structural characterization of the AB dimer from *Amphitrite ornata*. *Acta Crystallogr. D66*, 529–538.

(8) Belyea, J., Gilvey, L. B., Davis, M. F., Godek, M., Sit, T. L., Lommel, S. A., and Franzen, S. (2005) Enzyme function of the globin dehaloperoxidase from *Amphitrite ornata* is activated by substrate binding. *Biochemistry 44*, 15637–15644.

(9) Franzen, S., Belyea, J., Gilvey, L. B., Davis, M. F., Chaudhary, C. E., Sit, T. L., and Lommel, S. A. (2006) Proximal Cavity, Distal Histidine, and Substrate Hydrogen-Bonding Mutations Modulate the Activity of *Amphitrite ornata* Dehaloperoxidase. *Biochemistry 45*, 9085–9094.

(10) Franzen, S., Gilvey, L. B., and Belyea, J. L. (2007) The pH dependence of the activity of dehaloperoxidase from *Amphitrite ornata*. *Biochim. Biophys. Acta 1774*, 121–130.

(11) Franzen, S., Sasan, K., Sturgeon, B. E., Lyon, B. J., Battenburg, B. J., Gracz, H., Dumariah, R., and Ghiladi, R. (2012) Nonphotochemical Base-Catalyzed Hydroxylation of 2,6-Dichloroquinone by H_2O_2 Occurs by a Radical Mechanism. *J. Phys. Chem. B 116*, 1666–1676.

(12) Nienhaus, K., Deng, P., Belyea, J., Franzen, S., and Nienhaus, G. U. (2006) Spectroscopic Study of Substrate Binding to the Carbonmonoxy Form of Dehaloperoxidase from *Amphitrite ornata*. *J. Phys. Chem. B 110*, 13264–13276.

(13) Thompson, M. K., Davis, M. F., de Serrano, V., Nicoletti, F. P., Howes, B. D., Smulevich, G., and Franzen, S. (2010) Internal Binding of Halogenated Phenols in Dehaloperoxidase-hemoglobin Inhibits Peroxidase Activity. *Biophys. J. 99*, 1586–1595.

(14) Thompson, M. K., Ghiladi, R. A., and Franzen, S. (2012) The Dehaloperoxidase Paradox. *Biochim. Biophys. Acta 1842*, 578–588.

(15) Du, J., Sono, M., and Dawson, J. H. (2010) Functional Switching of *Amphitrite ornata* Dehaloperoxidase from O_2-Binding Globin to Peroxidase Enzyme Facilitated by Halophenol Substrate and H_2O_2. *Biochemistry 49*, 6064–6069.

(16) Osborne, R. L., Coggins, M. K., Raner, G. M., Walla, M., and Dawson, J. H. (2009) The Mechanism of Oxidative Halophenol Dehalogenation by *Amphitrite ornata* Dehaloperoxidase Is Initiated by H_2O_2 Binding and Involves Two Consecutive One-Electron Steps: Role of Ferryl Intermediates. *Biochemistry 48*, 4231−4238.
(17) Osborne, R. L., Taylor, L. O., Han, K. P., Ely, B., and Dawson, J. H. (2004) *Amphitrite ornata* dehaloperoxidase: Enhanced activity for the catalytically active globin using MCPBA. *Biochem. Biophys. Res. Commun. 324*, 1194−1198.
(18) Zhao, J. J., Rowe, J., Franzen, J., He, C., and Franzen, S. (2012) Study of the electrostatic effects of mutations on the surface of dehaloperoxidase-hemoglobin A. *Biochem. Biophys. Res. Commun. 420*, 733−737.
(19) Feducia, J., Dumarieh, R., Gilvey, L. B. G., Smirnova, T., Franzen, S., and Ghiladi, R. A. (2009) Characterization of Dehaloperoxidase Compound ES and Its Reactivity with Trihalophenols. *Biochemistry 48*, 995−1005.
(20) Thompson, M. K., Franzen, S., Ghiladi, R. A., Reeder, B. J., and Svistunenko, D. A. (2010) Compound ES of Dehaloperoxidase Decays via Two Alternative Pathways Depending on the Conformation of the Distal Histidine. *J. Am. Chem. Soc. 132*, 17501−17510.
(21) D'Antonio, J., and Ghiladi, R. A. (2011) Reactivity of Deoxy- and Oxyferrous Dehaloperoxidase B from *Amphitrite ornata*: Identification of Compound II and Its Ferrous-Hydroperoxide Precursor. *Biochemistry 50*, 5999−6011.
(22) Sturgeon, B. E., Battenburg, B. J., Lyon, B. J., and Franzen, S. (2011) Revisiting the Peroxidase Oxidation of 2,4,6-Trihalophenols: ESR Detection of Radical Intermediates. *Chem. Res. Toxicol. 24*, 1862−1868.
(23) Ator, M. A., David, S. K., and Demontellano, P. R. O. (1987) Structure and Catalytic Mechanism of Horseradish-Peroxidase: Regiospecific Meso-Alkylation of the Prosthetic Heme Group by Alkylhydrazines. *J. Biol. Chem. 262*, 14954−14960.
(24) Ferrari, R. P., Laurenti, E., and Trotta, F. (1999) Oxidative 4-dechlorination of 2,4,6-trichlorophenol catalyzed by horseradish peroxidase. *JBIC, J. Biol. Inorg. Chem. 4*, 232−237.
(25) Gumiero, A., Murphy, E. J., Metcalfe, C. L., Moody, P. C. E., and Raven, E. L. (2010) An analysis of substrate binding interactions in the heme peroxidase enzymes: A structural perspective. *Arch. Biochem. Biophys. 500*, 13−20.
(26) Macdonald, I. K., Badyal, S. K., Ghamsari, L., Moody, P. C. E., and Raven, E. L. (2006) Interaction of ascorbate peroxidase with substrates: A mechanistic and structural analysis. *Biochemistry 45*, 7808−7817.
(27) Sharp, K. H., Moody, P. C. E., Brown, K. A., and Raven, E. L. (2004) Crystal structure of the ascorbate peroxidase-salicylhydroxamic acid complex. *Biochemistry 43*, 8644−8651.
(28) LiCata, V. J., and Allewell, N. M. (1997) Is substrate inhibition a consequence of allostery in aspartate transcarbamylase? *Biophys. Chem. 64*, 225−234.
(29) Kühn-Velten, W. N., Bunse, T., and Förster, M. E. (1991) Enzyme kinetic and inhibition analyses of cytochrome P450XVII, a protein with a bifunctional catalytic site. Quantification of effective substrate concentrations at the active site and their significance for intrinsic control of the hydroxylase/lyase reaction sequence. *J. Biol. Chem. 266*, 6291−6301.
(30) Chaudhury, S., and Igoshin, O. A. (2009) Dynamic Disorder-Driven Substrate Inhibition and Bistability in a Simple Enzymatic Reaction. *J. Phys. Chem. B 113*, 13421−13428.
(31) Chen, Z., de Serrano, V., Betts, L., and Franzen, S. (2009) Distal histidine conformational flexibility in dehaloperoxidase from *Amphitrite ornata*. *Acta Crystallogr. D65*, 34−40.
(32) de Serrano, V., Chen, Z. X., Davis, M. F., and Franzen, S. (2007) X-ray crystal structural analysis of the binding site in the ferric and oxyferrous forms of the recombinant heme dehaloperoxidase cloned from *Amphitrite ornata*. *Acta Crystallogr. D63*, 1094−1101.
(33) de Serrano, V. S., Davis, M. F., Gaff, J. F., Zhang, Q., Chen, Z., D'Antonio, E. L., Bowden, E. F., Rose, R., and Franzen, S. (2010) X-ray structure of the metcyano form of dehaloperoxidase from *Amphitrite ornata*: Evidence for photoreductive dissociation of the iron-cyanide bond. *Acta Crystallogr. D66*, 770−782.
(34) Otwinowski, Z., and Minor, W. (1997) Processing of X-ray diffraction data collected in oscillation mode. *Methods Enzymol. 276*, 307−326.
(35) McCoy, A. J., Grosse-Kunstleve, R. W., Storoni, L. C., and Read, R. J. (2005) Likelihood-enhanced fast translation functions. *Acta Crystallogr. D61*, 458−464.
(36) Emsley, P., and Cowtan, K. (2004) Coot: Model-building tools for molecular graphics. *Acta Crystallogr. D60*, 2126−2132.
(37) Murshudov, G. N., Vagin, A. A., and Dodson, E. J. (1997) Refinement of macromolecular structures by the maximum-likelihood method. *Acta Crystallogr. D53*, 240−255.
(38) DeLano, W. L. (2002) *The PyMOL Molecular Graphics System*, DeLano Scientific LLC, San Carlos, CA.
(39) Engasser, J. M., and Horvath, C. (1974) Inhibition of Bound Enzymes. 3. Diffusion Enhanced Regulatory Effect with Substrate Inhibition. *Biochemistry 13*, 3855−3859.
(40) Brennan, S., and Cowan, P. L. (1992) A suite of programs for calculating X-ray absorption, reflection and diffraction performance for a variety of materials at arbitrary wavelengths. *Rev. Sci. Instrum. 63*, 850.
(41) Matthews, B. W. (1966) The Determination of the Position of Anomalously Scattering Heavy Atom Groups in Protein Crystals. *Acta Crystallogr. 20*, 230−239.
(42) Cromer, D. T., and Mann, J. B. (1968) X-ray Scattering Factors Computerd from Numerical Hartree-Fock Wave Functions. *Acta Crystallogr. A24*, 321−327.
(43) de Serrano, V., and Franzen, S. (2012) Structural Evidence for Stabilization of Inhibitor Binding by a Protein Cavity in the Dehaloperoxidase-Hemoglobin from *Amphitrite ornata*. *Pept. Sci. 98*, 27−35.
(44) LaCount, M. W., Zhang, E. L., Chen, Y. P., Han, K. P., Whitton, M. M., Lincoln, D. E., Woodin, S. A., and Lebioda, L. (2000) The crystal structure and amino acid sequence of dehaloperoxidase from *Amphitrite ornata* indicate common ancestry with globins. *J. Biol. Chem. 275*, 18712−18716.
(45) Lebioda, L., LaCount, M. W., Zhang, E., Chen, Y. P., Han, K., Whitton, M. M., Lincoln, D. E., and Woodin, S. A. (1999) An enzymatic globin from a marine worm. *Nature 401*, 445.
(46) D'Antonio, E. L., Bowden, E. F., and Franzen, S. (2012) Thin-layer spectroelectrochemistry of the Fe(III)/Fe(II) redox reaction of dehaloperoxidase-hemoglobin. *J. Electroanal. Chem. 668*, 37−43.
(47) de Serrano, V. S., Davis, M. F., Gaff, J. F., Zhang, Q., Chen, Z., D'Antonio, E. L., Bowden, E. F., Rose, R., and Franzen, S. (2010) X-ray structure of the metcyano form of dehaloperoxidase from *Amphitrite ornata*: Evidence for photoreductive dissociation of the iron-cyanide bond. *Acta Crystallogr. D66*, 770−782.
(48) Ma, H. A., Thompson, M. K., Gaff, J., and Franzen, S. (2010) Kinetic Analysis of a Naturally Occurring Bioremediation Enzyme: Dehaloperoxidase-Hemoglobin from *Amphitrite ornata*. *J. Phys. Chem. B 114*, 13823−13829.
(49) Davis, M. F., Bobay, B. G., and Franzen, S. (2010) Determination of Separate Inhibitor and Substrate Binding Sites in the Dehaloperoxidase-Hemoglobin from *Amphitrite ornata*. *Biochemistry 49*, 1199−1206.
(50) Davis, M. F., Gracz, H., Vendeix, F. A. P., de Serrano, V., Somasundaram, A., Decatur, S. M., and Franzen, S. (2009) Different Modes of Binding of Mono-, Di-, and Trihalogenated Phenols to the Hemoglobin Dehaloperoxidase from *Amphitrite ornata*. *Biochemistry 48*, 2164−2172.
(51) Nicoletti, F. P., Thompson, M. K., Howes, B. D., Franzen, S., and Smulevich, G. (2010) New insights into the role of distal histidine flexibility in ligand stabilization of dehaloperoxidase-hemoglobin from *Amphitrite ornata*. *Biochemistry 49*, 1903−1912.
(52) Osborne, R. L., Raner, G. M., Hager, L. P., and Dawson, J. H. (2006) *C. fumago* Chloroperoxidase Is also a Dehaloperoxidase: Oxidative Dehalogenation of Halophenols. *J. Am. Chem. Soc. 128*, 1036−1037.

(53) Nienhaus, K., Nickel, E., Davis, M. F., Franzen, S., and Nienhaus, G. U. (2008) Determinants of Substrate Internalization in the Distal Pocket of Dehaloperoxidase Hemoglobin of *Amphitrite ornata*. *Biochemistry 47*, 12985−12994.
(54) Thompson, M. K., Franzen, S., Davis, M. F., Oliver, R. C., and Krueger, J. K. (2011) Dehaloperoxidase-Hemoglobin from *Amphitrite ornata* Is Primarily a Monomer in Solution. *J. Phys. Chem. B 115*, 4266−4272.
(55) Kochanowska-Karamyan, A. J., and Hamann, M. T. (2010) Marine Indole Alkaloids: Potential New Drug Leads for the Control of Depression and Anxiety. *Chem. Rev. 110*, 4489−4497.
(56) Chen, X., Christopher, A., Jones, J. P., Bell, S. G., Guo, Q., Xu, F., Rao, Z., and Wong, L.-L. (2002) Crystal structure of the F87W-Y96F-V247L mutant of cytochrome P450cam with 1,3,5-trichlorobenzene bound and further protein engineering for the oxidation of pentachlorobenzene and hexachlorobenzene. *J. Biol. Chem. 277*, 37519−37526.
(57) Lin, Y., Lu, P., Tang, C., Mei, Q., Sandig, G., Rodrigues, A. D., Rushmore, T. H., and Shou, M. (2001) Substrate inhibition kinetics for cytochrome P450-catalyzed reactions. *Drug Metab. Dispos. 29*, 368−374.
(58) Sono, M., Roach, M. P., Coulter, E. D., and Dawson, J. H. (1996) Heme-containing oxygenases. *Chem. Rev. 96*, 2841−2887.
(59) Henricksen, A., Schuller, D. J., Meno, K., Welinder, K. G., Smith, A. T., and Gajhede, M. (1998) Structural interactions between horseradish peroxidase C and the substrate benzhydroxamic acid determined by X-ray crystallography. *Biochemistry 37*, 8054−8060.
(60) Weber, R. E., Mangum, C., Steinman, H., Bonaventura, C., Sullivan, B., and Bonaventura, J. (1977) Hemoglobins of two terebellid polychaetes: Enoplobranchus sanguineus and *Amphitrite ornata*. *Comp. Biochem. Physiol., Part A: Mol. Integr. Physiol. 56*, 179−187.
(61) Chen, Y. P., Woodin, S. A., Lincoln, D. E., and Lovell, C. R. (1996) An unusual dehalogenating peroxidase from the marine terebellid ploychaete *Amphitrite ornata*. *J. Biol. Chem. 271*, 4609−4612.
(62) Nicoletti, F. P., Thompson, M. K., Franzen, S., and Smulevich, G. (2011) Degradation of sulfide by dehaloperoxidase-hemoglobin from *Amphitrite ornata*. *JBIC, J. Biol. Inorg. Chem. 16*, 611−619.
(63) Vangberg, T., Bocian, D. F., and Ghosh, A. (1997) *JBIC, J. Biol. Inorg. Chem. 2*, 526−530.
(64) Osborne, R. L., Sumithran, S., Coggins, M. K., Chen, Y.-P., Lincoln, D. E., and Dawson, J. H. (2006) Spectroscopic characterization of the ferric states of *Amphitrite ornata* dehaloperoxidase and *Notomastus lobatus* chloroperoxidase: His-ligated peroxidases with globin-like proximal and distal properties. *J. Inorg. Biochem. 100*, 1100−1108.